

REVIEW

Micro-architected materials: past, present and future

BY N. A. FLECK*, V. S. DESHPANDE AND M. F. ASHBY

*Department of Engineering, University of Cambridge, Trumpington Street,
Cambridge, CB2 1PZ, UK*

Micro-architected materials offer the opportunity of obtaining unique combinations of material properties. First, a historical perspective is given to the expansion of material property space by the introduction of new alloys and new microstructures. Principles of design of micro-architecture are then given and the role of nodal connectivity is emphasized for monoscale and multi-scale microstructures. The stiffness, strength and damage tolerance of lattice materials are reviewed and compared with those of fully dense solids. It is demonstrated that micro-architected materials are able to occupy regions of material property space (such as high stiffness, strength and fracture toughness at low density) that were hitherto empty. Some challenges for the development of future materials are highlighted.

Keywords: lattice materials; foams; mechanical properties

1. Introduction: a materials time-line

In this paper, the evolution of engineering materials is outlined with the main enablers of change. The history of this evolution is illustrated in the first two sections of the paper, introducing the concept of *material property space*. Strategies are identified for filling the remaining gaps of this space. The ability of micro-architected lattice materials to give a wide range of stiffness, strength and fracture toughness is described, with the role of nodal connectivity and structural hierarchy emphasized. The damage tolerance of lattice materials relative to that of the parent solid is then discussed with an identification of several transition flaw sizes. Finally, some future directions are given for the future development of lattice materials, and the utility of cross-property relations and bounding theorems is discussed.

Figure 1 is a materials time-line. It is interesting to follow its development, starting from the bottom and working upwards. The tools and weapons of prehistory, 300 000 or more years ago, were bone and stone. Stones could be

*Author for correspondence (naf1@eng.cam.ac.uk).

One contribution to the 2010 Anniversary Series ‘A collection of reviews celebrating the Royal Society’s 350th Anniversary’.

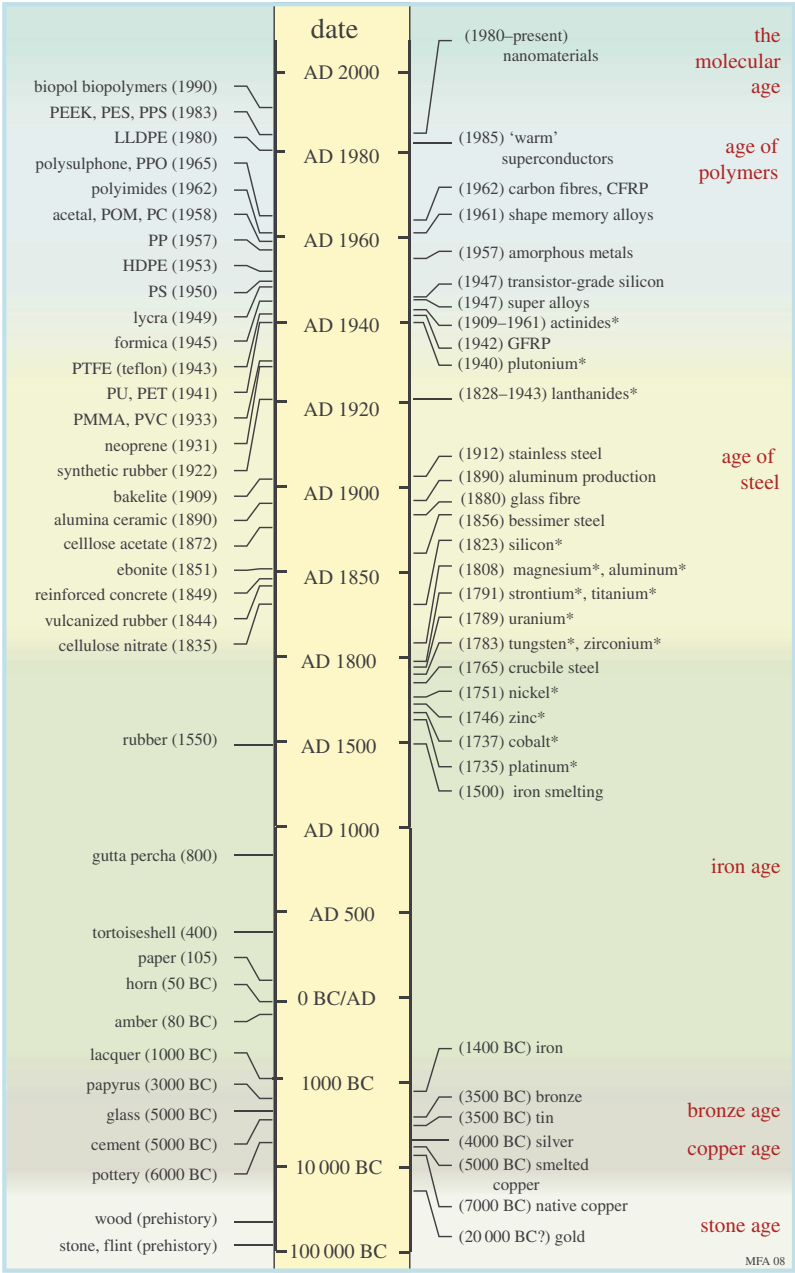


Figure 1. A materials time-line. The scale is nonlinear, with big steps at the bottom, small ones at the top. An asterisk indicates the date at which an element was first identified. Labels without an asterisk give the date at which the material became of practical importance. PEEK, poly ether ether ketone; PES, poly ether sulfone; PPS, poly phenylene sulphide; LLDPE, linear low-density polyethylene; PPO, polyphenylene oxide; POM, polyoxymethylene; PC, polypropylene; HDPE, high-density polyethylene; PS, polystyrene; PTFE, polytetrafluoroethylene; PU, polyurethane; PET, polyethylene terephthalate; PMMA, polymethyl methacrylate; PVC, polyvinyl chloride; CFRP, carbon fibre reinforced polymer; GFRP, glass fibre reinforced polymer.

shaped for tools, particularly flint and quartz, which can be flaked to produce a cutting edge that was harder, sharper more durable than any other material that could be found in nature. Gold, silver and copper, the only metals that occur in native form, must have been known from the earliest time, but the realization that they were ductile, could be beaten to complex shape, and—once beaten—became hard, seems to have occurred around 5500 BC. By 4000 BC, there is evidence that the technology to melt and cast these metals had developed, allowing more intricate shapes. Native copper, however, is not abundant. Copper occurs in far greater quantities as the minerals azurite and malachite. By 3500 BC, kiln furnaces, developed for pottery, could reach the temperature required for the reduction of these minerals, making copper sufficiently plentiful to be used for implements and weapons. But even in the worked state, copper is relatively soft. Around 3000 BC, the accidental inclusion of a tin-based mineral, cassiterite, in the copper ores provided the next step in technology—the production of the alloy *bronze*, a mixture of tin and copper, with a strength and hardness that pure copper cannot match.

The discovery, around 1450 BC, of ways to reduce ferrous oxides to make iron, a material with greater stiffness, strength and hardness than any other then available, rendered bronze obsolete. Iron was not entirely new: tiny quantities existed as the cores of meteors that had impacted the Earth. By contrast, the oxides of iron are widely available, particularly *hematite*, Fe_2O_3 . Hematite is easily reduced by carbon, although it takes high temperatures, close to 1100°C , to do it. This temperature is insufficient to melt iron, so the material produced was a spongy mass of solid iron intermixed with slag; this was reheated and hammered to expel the slag and then forged into the desired shape. The casting of iron was a more difficult challenge, requiring temperatures of around 1600°C . Two millennia passed before, in AD 1500, the blast furnace was developed, enabling the widespread use of cast iron. Cast iron allowed structures of a new type: the great bridges, railway terminals and civil buildings of the early nineteenth century are testimony to it. But it was steel, made possible in industrial quantities by the Bessemer process of 1856, that gave iron its dominant role in structural design that it still holds today.

The demands of the expanding aircraft industry in the 1950s shifted emphasis to the light alloys (those of aluminium, magnesium and titanium) and to materials that could withstand the extreme temperatures of the turbine combustion chamber. The development of superalloys—heavily alloyed iron, nickel and cobalt-based materials—became the focus of research, delivering an extraordinary range of alloys able to carry load at temperatures above 1200°C . The range of their applications expanded into other fields, particularly those of chemical and petroleum engineering.

The history of polymers is rather different. Wood, of course, is a polymeric composite, one used for construction from the earliest times. The beauty of amber—petrified resin—and of horn and tortoise shell—the polymer *keratin*—already attracted designers from the earliest times. Rubber, brought to Europe in 1550, grew in importance in the nineteenth century, partly because of the wide spectrum of properties made possible by vulcanization—cross-linking by sulphur—giving materials as elastic as latex or as rigid as ebonite. The real polymer revolution, however, has its beginnings in the early twentieth century with the development of Bakelite, a phenolic, in 1909 and synthetic

butyl rubber in 1922. This was followed, in mid-century, by a period of rapid development of polymer science. Almost all the polymers we use so widely today were developed in a 20 year span from 1940 to 1960, among them the bulk commodity polymers polypropylene, polyethylene, polyvinyl chloride and polyurethane, the combined annual tonnage of which now approaches that of steel. Design with polymers has matured: they are now as important as metals in household products, automobiles and, most recently, in aerospace. Unreinforced polymers lack the stiffness and strength many of these applications demand. They are used, instead, as *composites*, reinforced with fillers and fibres. Composite technology is not new. Straw-reinforced mud brick is one of the earliest of the materials of architecture and remains one of the traditional materials for building in parts of Africa and Asia, even today. Steel-reinforced concrete—the material of shopping centres, road bridges and apartment blocks—appeared just before 1850. The reinforcement of polymers was enabled by the technology for making glass fibres, which had existed since 1880. Glass wool, or better, woven or layered glass fibres, could be incorporated in thermosetting polyesters or epoxies, giving them the stiffness and strength of aluminium alloys. By the mid-1940s, glass fibre reinforced polymer components were in use in the aircraft industry. The real transformation of polymers into high-performance structural materials came with the development of aramid and carbon fibres in the 1960s. Incorporated as reinforcements, they give materials with performance (meaning stiffness and strength per unit weight) which exceeded that of all other bulk materials, giving them their now-dominant position in high-performance sports equipment and aerospace.

The period in which we now live might have been named the polymers and composites era had it not coincided with a second revolution that is based on silicon. Silicon was first identified as an element in 1823, but found few uses until the discovery, in 1947, that, when doped with tiny levels of impurity, it could act as a rectifier. The discovery has created the fields of electronics, mechatronics and modern computer science, revolutionizing information storage, access and transmission, imaging, sensing and actuation, numerical modelling and much more. This is rightly called the information age, enabled by the development of transistor-grade silicon.

In the last two decades, the area of biomaterials has developed rapidly. Implanting materials in or on the human body was not practical until the aseptic surgical technique was developed in the late 1800s. Non-toxic metal alloys were introduced, but tended to fracture in service. It was not until the development of polymer-based systems, and subsequently, with a new wave of discoveries in cell biology, chemistry and materials science, that synthetic biomaterials became a reality.

During the early 1990s, it was realized that material behaviour depended on scale, and that the dependence was most evident when the scale was that of nanometres. Although the term nanoscience is new, the use of nanotechnology is not. The proteins and minerals of soft and mineralized tissue in plants and animals are dispersed on a nano-scale. Nanoparticles of carbon have been used for the reinforcement of tyres. The light alloys of aerospace derive their strength from a nano-scale dispersion of precipitates. Modern nanotechnology gained prominence with the discovery of various forms of carbon such as the C60

molecule and carbon nanotubes, though even these are not really new but have always existed as particles in smoke. True nano-engineering has finally come with the development of tools capable of resolving and manipulating matter at the atomic level, making it possible (though at present expensive) to build materials and structures the way nature does it, atom by atom and molecule by molecule.

Figure 1 tracks the expanding portfolio of materials available to the engineer. With it comes an expansion of the accessible range of stiffness, strength and toughness. The expansion of one of these—strength—is illustrated in the next section.

2. Expanding the boundaries of material property space

The material development documented in the time-line were driven by the desire for ever greater performance. One way of examining the progress of this is by following the way in which properties have evolved on *material property charts*. Material property charts (Ashby 2010) display materials on axes based on two of their properties. Materials have many properties of course (mechanical, thermal, electrical, optical, etc.) and so the number of such pair-wise combinations is large. Each chart can be thought of as a slice through ‘material property space’—a multi-dimensional space with material properties as its axes.

Figure 2 is an example of just one of them. It is a *strength–density chart*. There are many obvious incentives for seeking materials with greater strength: more durable and effective tools and weapons; faster, more economical transport; and larger, more daring structures. In more recent times, it has been high strength at low weight that is frequently sought, with transport and aerospace as the direct drivers.

The chart is plotted for six successive points in historical time, ending with the present day. The materials of pre-history, shown in figure 2*a*, cover only a tiny fraction of this strength–density space. By the time of the peak of the Roman empire, around 50 BC (figure 2*b*), the area occupied by metals has expanded considerably. The progress thereafter was slow: 1500 years later (figure 2*c*) not much has changed, although, significantly, cast iron now appears. Even 500 years after that (figure 2*d*), expansion of the occupied area of the chart is small; aluminium only just creeps in. Then things accelerate. By 1945, the metals envelope has expanded considerably and a new envelope—that of synthetic polymers—now occupies a significant position. Between then and the present day the expansion has been dramatic. How much further can we go? That is a question we explore in the sections that follow.

3. Strategies for filling material property space

Material property charts each have the feature that parts of them are populated with materials and parts are not—there are holes. Some parts are inaccessible for fundamental reasons that relate to the size of atoms and the nature of the forces that bind them together. But other parts are empty even though, in principle, they could be filled.

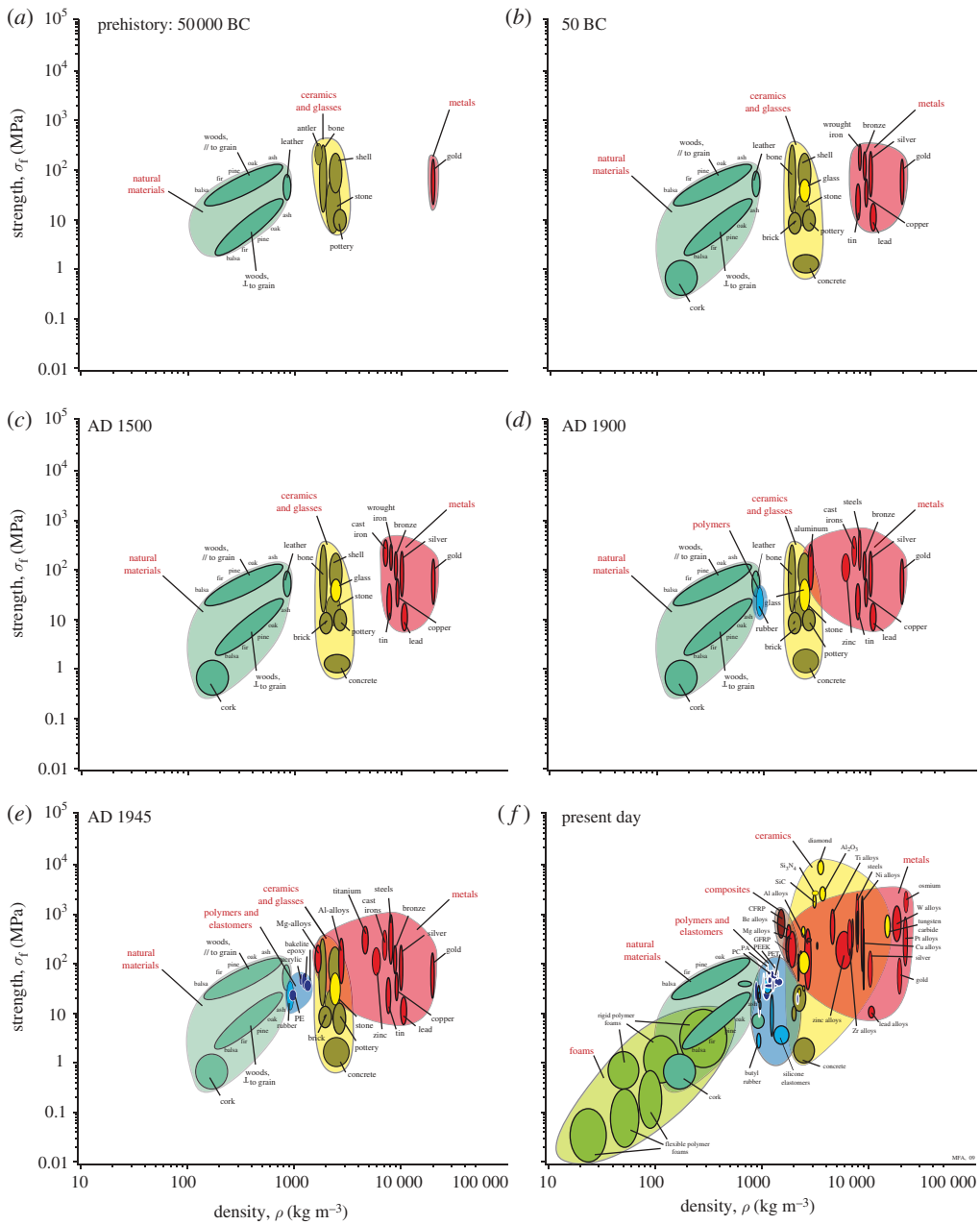


Figure 2. The progressive filling of material property space over time (the charts list the date at the top left)—here the way the materials have been developed over time to meet demands on strength and density. Similar time plots show the progressive filling of similar plots for all material properties. PE, polyethylene; CFRP, carbon fibre reinforced polymer; GFRP, glass fibre reinforced polymer; PEEK, poly ether ether ketone; PA, polyamide; PC, polycarbonate; PET, polyethylene terephthalate.

One approach to filling holes in material property space is that of manipulating *chemistry*, developing new metal alloys, new polymer formulations and new compositions of glass and ceramic, which extends the populated areas of the property charts. A second is that of manipulating *microstructure*, using thermo-mechanical processing to control the distribution of phases and defects within materials. Both have been exploited systematically, leaving little room for further gains, which tend to be incremental rather than step like. A third approach is that of controlling *architecture* to create hybrid materials—combinations of materials or of material and space in configurations and with connectivities that offer enhanced performance. The success of carbon and glass-fibre reinforced composites at one extreme, and of foamed materials at another, in filling previously empty areas of the property charts is encouragement enough to explore this route in greater depth. In the present study, we limit attention to the extreme case of porous solids (a hybrid of the solid and air), and explore the effect of micro-architecture upon properties.

(a) *Lattice materials*

We define a general *lattice material* as a cellular, reticulated, truss or lattice structure made up of a large number of uniform lattice elements (e.g. slender beams or rods) and generated by tessellating a unit cell, comprised of just a few lattice elements, throughout space. Here, we use the term ‘material’ to emphasize that we shall consider lattices with global, macroscopic length scales much larger than that characteristic of their constituent lattice elements (e.g. individual rod length). For the lattice to behave as a material, the wavelength of any loading is also much longer than that of the lattice elements. In contrast, the lattice behaves as a ‘structure’ when it contains a relatively small number of lattice elements, and the length scale of the loading is comparable to that of the lattice elements.

Classically, periodic *planar lattices* are classified as *regular*, *semi-regular* or other. *Regular lattices* are generated by tessellating a regular polygon to fill the entire plane (Cundy & Rolett 1961; Lockwood & Macmillan 1978; Frederickson 1997). Only a few regular polygons produce such a lattice: these are the triangle, square and hexagon, with sketches of the triangulated and hexagonal lattice included in figure 3. *Semi-regular lattices* are generated by tessellating two or more different kinds of regular polygons to fill the entire plane (Cundy & Rolett 1961; Lockwood & Macmillan 1978; Frederickson 1997). It may be shown that there exist only eight, independent, such lattices and no more. An example of such a lattice is the ‘triangular–hexagonal’ lattice, also known as the *Kagome* lattice (Syozi 1972; Hyun & Torquato 2002). Additional plane-filling lattices can be constructed from two or more polygons of different size, or by relaxing the restriction that each joint has the same connectivity (e. g. Hutchinson 2004).

Spatial or three-dimensional lattices can be generated by filling space from polyhedra. Of the regular polyhedra with a small number of faces, only the cube and the rhombic dodecahedra can be tessellated to fill all space (Gibson & Ashby 1997). Typically, spatial lattices are constructed using combinations of different polyhedra, for example, tetrahedra and octahedra may be packed to form the octet-truss lattice (Deshpande *et al.* 2001a).

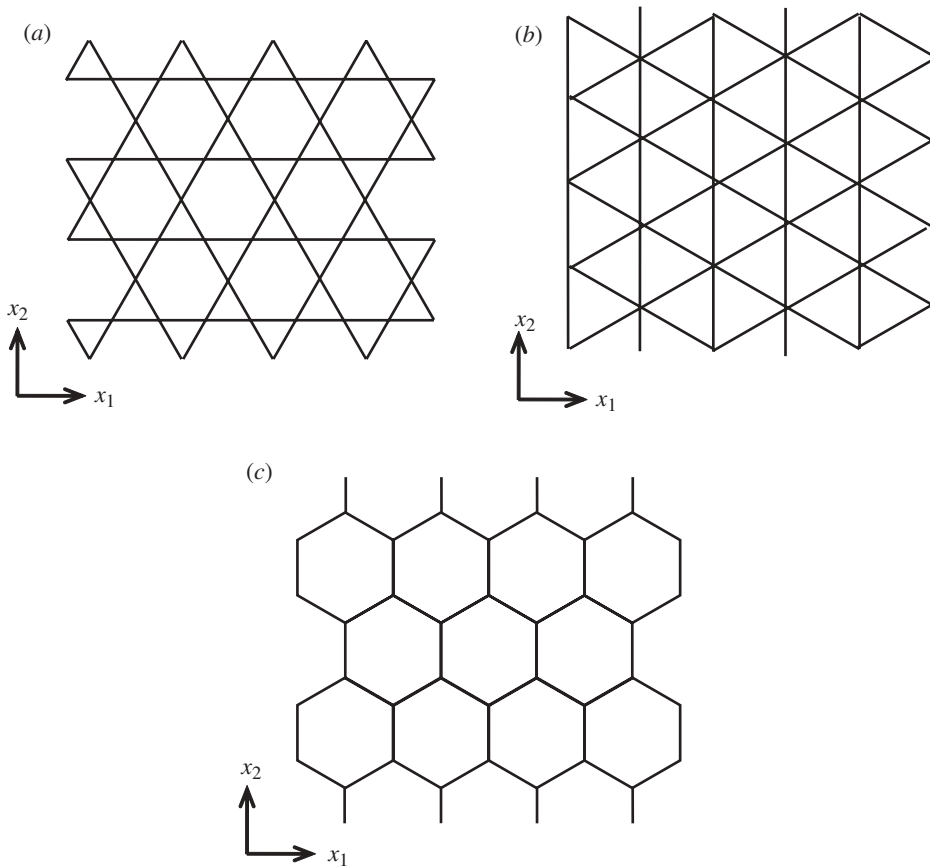


Figure 3. (a) Kagome lattice, (b) triangular lattice and (c) hexagonal lattice.

In the following, we shall argue that the properties of lattice materials are dictated by the volume fraction of cell-wall material and also by the nodal connectivity: the number of struts that meet at each node of the microstructure.

4. Expanding property space by the design of lattice materials

The relative density $\bar{\rho}$ of a lattice material is defined as the ratio of the density of the lattice material to the density of the solid. Lattice materials resemble frameworks when $\bar{\rho}$ is less than about 0.2, and in this regime $\bar{\rho}$ is directly related to the thickness t and length ℓ of a strut according to

$$\bar{\rho} = A \left(\frac{t}{\ell} \right) \quad (4.1)$$

for a two-dimensional lattice. The constant of proportionality A depends upon the geometry: for the hexagonal, Kagome and fully triangulated lattices as shown in figure 3, we find that A equals $2/\sqrt{3}$, $\sqrt{3}$ and $2\sqrt{3}$, respectively, as listed in table 1.

Table 1. Coefficients for the scaling laws.

topology	A	B	b	ν	C	c	D	d
hexagonal	$2/\sqrt{3}$	$3/2$	3	1	$1/3$	2	0.90	2
triangular	$2\sqrt{3}$	$1/3$	1	$1/3$	$1/3$	1	0.61	1
Kagome	$\sqrt{3}$	$1/3$	1	$1/3$	$1/2$	1	0.21	$1/2$

A three-dimensional lattice or foam can be either open or closed celled as follows. *Open-cell* microstructures comprise a three-dimensional arrangement of inter-connected struts, and have the property that $\bar{\rho}$ scales with $(t/\ell)^2$. *Closed-cell* microstructures also exist, with plate-like cell faces of thickness t and side length ℓ ; their relative density scales with (t/ℓ) , provided the cell faces have uniform thickness. Closed-cell foams, typically, have thickened cell edges; giving a dependence of $\bar{\rho}$ on (t/ℓ) between these two extremes.

(a) The role of nodal connectivity

There are two distinct species of cellular solid. The distinction is most obvious in their mechanical properties. The first, typified by foams, are *bending-dominated structures*; the second, typified by triangulated lattice structures, are *stretching-dominated structures*—a distinction explained more fully below, and detailed in Deshpande *et al.* (2001*b*). To give an idea of the difference: a foam with a relative density of 0.1 (meaning that the solid cell walls occupy 10% of the volume) is less stiff by a factor of 3 than a triangulated lattice of the same relative density. The macroscopic properties are largely dictated by the connectivity of joints rather than by the regularity of the microstructure.

The distinction of a bending-dominated structure and a stretching-dominated microstructure structure is closely linked to the collapse response of a pin-jointed structure of the same morphology. If the parent pin-jointed lattice exhibits collapse mechanisms that generate macroscopic strain, then the welded-joint version relies upon the rotational stiffness and strength of the nodes and struts for its macroscopic behaviour: consequently, the parent lattice is bending dominated. In contrast, when the parent lattice has only periodic collapse mechanisms or no collapse mechanisms, the welded-joint version is stretching governed. In broad terms, the type of response is dependent upon the nodal connectivity.

Maxwell analysed a pin-jointed frame (meaning one that is hinged at its corners) made up of b struts and j frictionless joints, like those in figure 3. He showed that a two-dimensional *statically* and *kinematically determinate* frame (one that is just rigid and does not fold up when loaded) has the property that

$$b - 2j + 3 = 0. \quad (4.2)$$

In a three-dimensional frame, the equivalent equation is

$$b - 3j + 6 = 0. \quad (4.3)$$

A generalization of the Maxwell rule in three-dimensional space is given by Calladine (1978) as follows:

$$b - 3j + 6 = s - m, \quad (4.4)$$

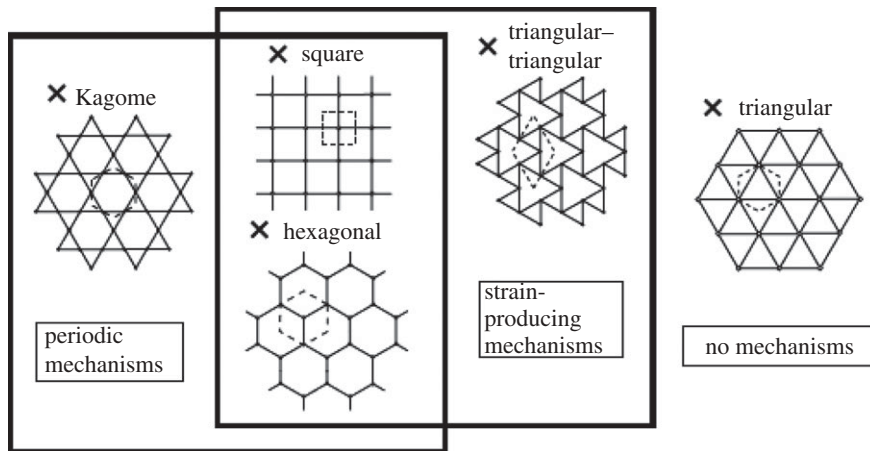


Figure 4. Venn diagram for selected two-dimensional lattices.

where s and m count the states of self-stress and mechanisms, respectively, and each can be determined by finding the rank of the equilibrium matrix that describes the frame in a full structural analysis (Pellegrino & Calladine 1986). A just rigid framework (i.e. a framework that is both statically and kinematically determinate) has $s = m = 0$. The nature of Maxwell's rule as a necessary rather than sufficient condition is made clear by examination of equation (4.2): vanishing of the LHS in equation (4.2) only implies that the number of mechanisms and states of self-stress are equal, not that each equals zero. If $m > 0$, then the frame contains *mechanisms*. It has no stiffness or strength; it collapses if loaded. If its joints are locked, preventing rotation (as they are in a lattice), the bars of the frame *bend*. If, instead, $m = 0$, then the frame ceases to be a mechanism. If it is loaded, its members carry tension or compression (even when pin jointed), and it becomes a *stretch-dominated* structure. Locking the hinges now makes little difference because slender structures are much stiffer when stretched than when bent.

We now turn our attention to a large pin-jointed framework of connectivity Z and j joints: the total number of bars b is approximately $jZ/2$. The necessary, but not sufficient, condition for rigidity is $Z = 4$ in two-dimensional space and $Z = 6$ in three-dimensional space (Deshpande *et al.* 2001*b*). A Venn diagram to illustrate the various types of mechanism exhibited by classes of a two-dimensional periodic pin-jointed truss is given in figure 4. Consider the various structures in turn. The fully triangulated structure, comprising equilateral triangles with a nodal connectivity of $Z = 6$, is highly redundant and possesses no collapse mechanisms. In contrast, a triangular-triangular lattice, with unit cell shown in figure 4, collapses by a mechanism that leads to a macroscopic hydrostatic strain. Thus, this structure has zero macroscopic stiffness against this collapse mode. The Kagome microstructure has a connectivity of $Z = 4$ and has no strain-producing collapse mechanisms; it can only collapse by periodic mechanisms that do not produce a macroscopic strain. Consequently, it is rigid in all directions. The cases of the square lattice and the hexagonal lattice, with a connectivity of $Z = 4$ and $Z = 3$, respectively, are different. Each of these structures can collapse by macroscopic strain-producing mechanisms, and by periodic collapse

mechanisms. A methodology has been developed by Hutchinson & Fleck (2005) to explore the periodic collapse mechanisms based on Bloch-wave analysis; the details are beyond the scope of the present article. The main conclusion to draw from figure 4 is that the fully triangulated structure is macroscopically stiff because it possesses no collapse mechanisms, while the Kagome structure is macroscopically stiff because it has only periodic collapse mechanisms that generate no macroscopic strain.

(b) *The in-plane stiffness of two-dimensional isotropic lattice materials*

Material property space can be expanded by suitable design of material architecture. To illustrate this, consider the in-plane properties of two-dimensional isotropic lattice materials: the hexagonal, Kagome and triangular lattices of nodal connectivity 3, 4 and 6, respectively, as sketched in figure 3. We begin by reviewing briefly the macroscopic in-plane stiffness of these two-dimensional lattices. Simple beam theory can be used to determine the effective, macroscopic Young modulus E and Poisson ratio ν of the lattices in terms of the relative density $\bar{\rho}$ and the Young modulus of the solid E_S . The scaling law can be adequately represented by the power-law expression

$$\frac{E}{E_S} = B\bar{\rho}^b, \quad (4.5)$$

where the values of the coefficient B and exponent b are listed in table 1. The Poisson ratio ν is independent of relative density, assuming it is sufficiently low for beam theory to be adequate in characterizing the behaviour of the lattice material. But ν does depend upon geometry, as summarized in table 1. The hexagonal lattice is bending dominated, with $b=3$. In contrast, the Kagome and fully triangulated lattices are stretching dominated, with $b=1$. Remarkably, the coefficient B and the Poisson ratio are also identical for the triangulated and Kagome lattices: these lattices have identical effective properties, and each achieves the Hashin–Shtrikman upper bound. The differences between the two lattices do show up however when imperfections are introduced. For example, by randomly perturbing the location of the nodes at fixed relative density, there is a large drop in the modulus of the Kagome lattice, but a much smaller drop in the modulus of the triangulated lattice (Romijn & Fleck 2007). This is due to the fact that the triangulated lattice has a higher nodal connectivity of $Z=6$ than that of the Kagome lattice ($Z=4$) and is a much more redundant structure when the struts are assumed to be pin jointed at the nodes. The role of imperfection for these two lattices is further explored below for the property of fracture toughness.

(c) *The strength of two-dimensional lattice materials*

Beam theory can also be used to determine the macroscopic fracture strength of the perfect lattice, in the absence of heterogeneities such as a macroscopic crack. Consider the lattices of figure 3 loaded macroscopically by a uniform in-plane stress. The lattice responds in a linear-elastic manner, with a stress state within each bar given by simple beam theory. Define failure of the lattice as the point at which the maximum local tensile stress within the lattice attains the tensile fracture strength of the solid σ_{TS} . The corresponding macroscopic stress defines the fracture strength of the lattice. None of the three lattices of figure 3

possess an isotropic fracture strength—the macroscopic tensile strength of the lattice varies with the direction of loading. However, Gibson & Ashby (1997) have shown that the degree of anisotropy is small. For definiteness, we review here the macroscopic uniaxial strength σ_c of the lattice, upon loading along the x_2 direction as shown in figure 3. The strength σ_c can be expressed in terms of the tensile fracture strength of the solid σ_{TS} as follows:

$$\frac{\sigma_c}{\sigma_{TS}} = C\bar{\rho}^c, \quad (4.6)$$

with the coefficients (C, c) dependent upon geometry, as listed in table 1. The triangular and Kagome structures deform by bar stretching, and this leads to $c = 1$, while the hexagonal honeycomb deforms by bar bending, giving $c = 2$.

(d) Three-dimensional lattices and foams

Now consider the case of open-cell metallic foams, as reviewed by Ashby *et al.* (2000). They are manufactured mostly from the melt by the expansion of gas bubbles, and the expansion process is driven by the minimization of surface energy. Consequently, they have microstructures that, although stochastic, have a low nodal connectivity of 3–4 adjoining bars per joint. The stiffness and strength of these three-dimensional structures relies upon the bending stiffness of the bars, and they are consequently referred to as *bending-dominated structures*. It follows from beam-bending theory and dimensional analysis that the Young modulus E of open-cell foams scales with that of the fully dense solid E_S according to $E \approx \bar{\rho}^2 E_S$. The yield strength σ_Y scales with $\bar{\rho}$ and with the yield strength of the parent solid σ_{YS} according to $\sigma_Y \approx 0.3\bar{\rho}^{3/2}\sigma_{YS}$. Both relations are supported by a wealth of experimental data (see Ashby *et al.* 2000). In contrast, the octet truss, identical in crystal structure to face-centred cubic, has a nodal connectivity (coordination number) of 12 and is a *stretching-dominated structure*. Stretching-dominated microstructures have the property that their Young modulus E and their yield strength σ_Y scale linearly with relative density $\bar{\rho}$, such that $E \approx 0.3\bar{\rho}E_S$ and $\sigma_Y \approx 0.3\bar{\rho}\sigma_{YS}$. (These values are of the order of the Hashin–Shtrikman upper bound for an isotropic solid.) Such lattice materials have the virtue that the stiffness and strength scale linearly with the relative density and thereby outperform metallic foams. A variety of fabrication routes have evolved to construct these periodic lattices (see Wadley *et al.* 2003).

It is instructive to display bending-dominated foams and stretching-dominated lattice materials in property space using the axes of E versus density and σ_Y versus density (see figure 5). The properties of the lattice materials scale linearly with density from that of the parent material, and fill-in some of the gaps of material property space. In contrast, the stiffness and strength of foams degrade at a faster rate than linearly with a decrease in density.

5. Multi-scale lattice materials

Nature makes use of *multi-scale* lattice materials, such that the material within each strut of the lattice comprises a lattice on a successively smaller scale (Ashby 1991, 2010). One reason for such structural hierarchy in engineering structures

is to increase buckling strength: recall that the buckling strength scales with any representative strut length ℓ according to ℓ^{-2} , and so the finer the length scale, the higher the buckling strength.

Nature frequently designs *compliant structures* that have sufficiently low moduli that low stresses are generated upon deformation, and the structures do not fail. Soft tissue is of this type: skin, cartilage and elastin, along with many types of bird's nests such as the woven Weaver bird's nest. One way of achieving low stiffness is to use structural hierarchy with a bending-dominated structure on various length scales.

Consider as a prototypical example a lattice material with struts (labelled 1) on a large scale made in turn from another lattice material with struts on a fine scale (labelled 2), as sketched in figure 6. The effective modulus E_2 of the fine-scale struts scales with the modulus E_S and relative density of the fine-scale struts $\bar{\rho}_2$ according to

$$E_2 = B_2 \bar{\rho}_2^{b_2} E_S. \quad (5.1)$$

Now construct the larger scale lattice material such that its struts are made from the fine-scale lattice of modulus E_2 . With the volume fraction of strut material 2 in the lattice material 1 written as $\bar{\rho}_1$, we note that the relative density of lattice material 1 to the solid is $\bar{\rho} = \bar{\rho}_1 \bar{\rho}_2$. Also, the effective modulus of the coarse-scale lattice E_1 is

$$E_1 = B_1 \bar{\rho}_1^{b_1} E_2 = B_1 B_2 \bar{\rho}_1^{b_1} \bar{\rho}_2^{b_2} E_S, \quad (5.2)$$

and for the case $b_1 = b_2$, this simplifies to

$$E_1 = B_1 B_2 \bar{\rho}^{b_1} E_S. \quad (5.3)$$

Now consider some examples from nature where the large-scale lattice 1 is a bending or stretching structure and the finer-scale lattice 2 (making up the struts of the larger lattice) is a bending or stretching structure. We consider each case in turn.

(a) Case I: a stretching–stretching structure

When both lattices have sufficient nodal connectivity that they are stretching-dominated in behaviour, we have $b_1 = b_2 = 1$ and the overall modulus E_1 is high. An example of this is the axial stiffness of woods: the cell walls are arranged as hexagonal prisms and, along the prismatic direction, the macro-lattice undergoes plate stretching. On a finer scale, each cell wall contains long fibres of cellulose and these too undergo stretching.

(b) Case II: a bending–bending structure

Highly compliant lattices can be made by exploiting bending of the primary struts of the lattice, along with the use of compliant cell-wall material (bending-dominated deformation of the finer-scale lattice). For an open-cell foam-like structure on both lengths scales, we have $b_1 = b_2 = 2$. Consider as an example, birds nests that have been made by weaving together the leaves of grass. The grass leaves are wavy and bend when the nest is deformed. And on a finer-scale

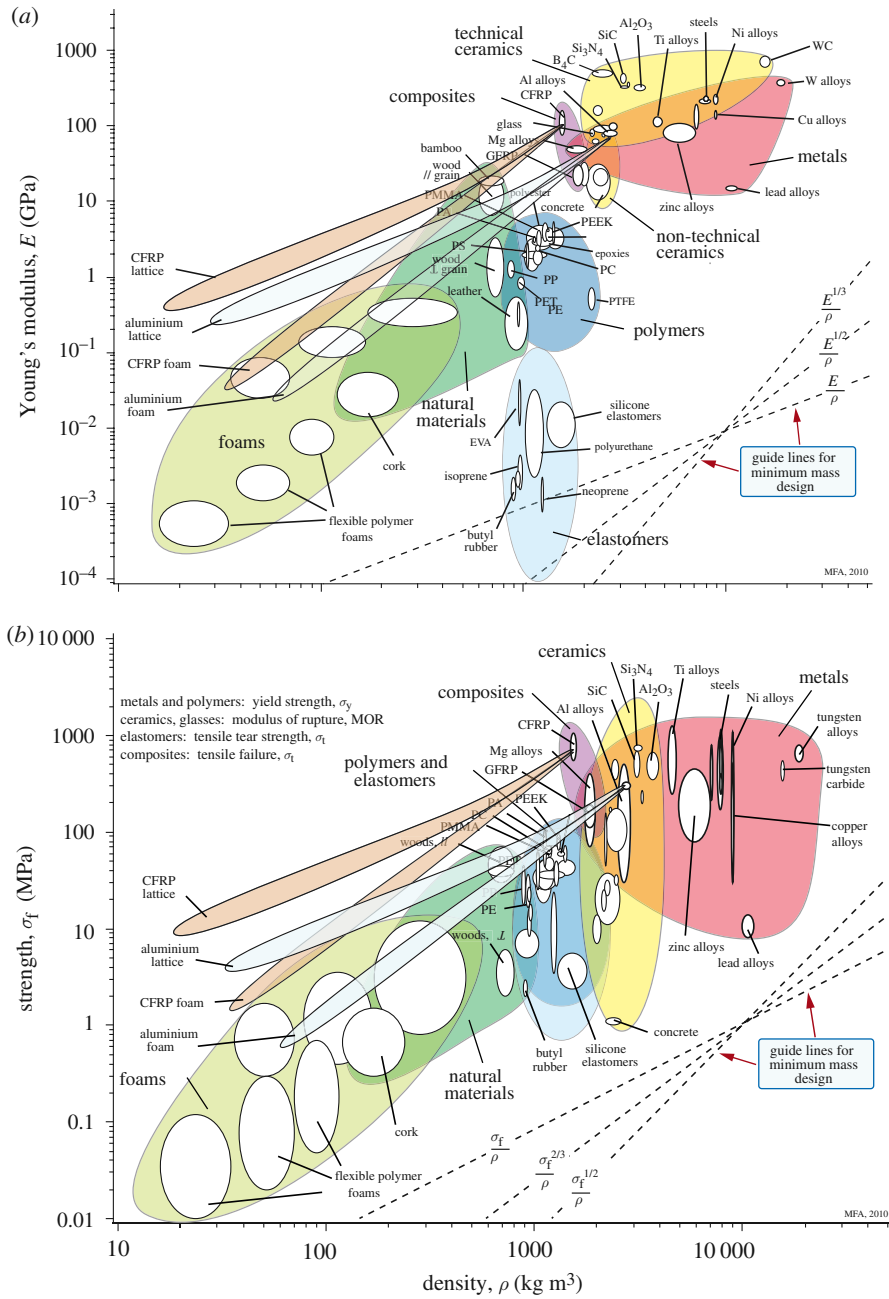


Figure 5. Material property charts of (a) E versus ρ and (b) σ_Y versus ρ for engineering materials. Predictions for bending-dominated foams and stretching-dominated lattices of CFRP and aluminium are superimposed. Lattices expand the occupied area of both charts. PMMA, polymethyl methacrylate; PA, polyamide; PEEK, poly ether ether ketone; PS, polystyrene; PP, polypropylene; PET, polyethylene terephthalate; PE, polyethylene; PC, polycarbonate; PTFE, polytetrafluoroethylene; CFRP, carbon fibre reinforced polymer; EVA, ethylene vinyl acetate.

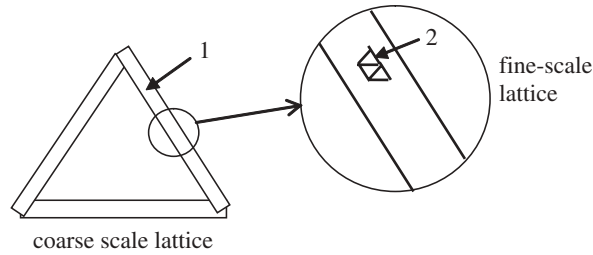


Figure 6. A hierarchical lattice on two length scales.

lattice, the grass is composed of a three-dimensional foam-like arrangement of cells with wavy sides. At this structural level too the cell walls bend under an imposed straining of the grass leaf. Consequently, the nest has a very low effective modulus. This is useful in making the nest damage tolerant during tropical storms.

(c) Case III: a stretching–bending structure

The intermediate case of a stretching-dominated lattice on one length scale and a bending-dominated lattice on a finer (or coarser) scale is also present in nature. Consider first the example of the transverse modulus of wood. On a coarse scale, the microstructure comprises a two-dimensional hexagonal lattice of wood cells, and the transverse modulus is dictated by bending of the cell walls, giving $b_1 = 3$. Bending of the cell walls involves stretching of the cellulose fibres within each cell wall, implying that $b_2 = 1$, and so the overall effective modulus is a result of bending on the coarse scale and stretching on the fine scale.

Second, consider a bird's wing that comprises a sandwich panel with solid faces and core struts. On the coarse scale, the struts undergo stretching ($b_1 = 1$), while on a finer scale, they comprise a three-dimensional foam-like microstructure that undergoes bending ($b_2 = 2$). The spectrin-based cytoskeleton on the cytosolic side of the human red blood cell membrane is another example of a stretching–bending structure. On the coarse scale, the spectrin is a fully triangulated, stretching-dominated lattice covering the cell membrane, whereas the spectrin fibres are elastomeric with a low modulus.

6. The fracture toughness of lattice materials

The fracture toughness of lattice materials can be calculated upon assuming that the individual struts behave as elastic–brittle beams and fail when the maximum local tensile stress at any point in the lattice attains the solid strength σ_f . Consider a finite lattice domain surrounding the tip of a macroscopic crack (see figure 7). The displacements \mathbf{u} and material rotation ψ of the beam ends are prescribed on the outer boundary according to the asymptotic K -field of a crack in an equivalent homogenous material possessing the effective elastic properties. The fracture toughness of the lattice is the value of applied stress intensity factor K such that the maximum local tensile stress attains the value σ_f . This formulation, referred

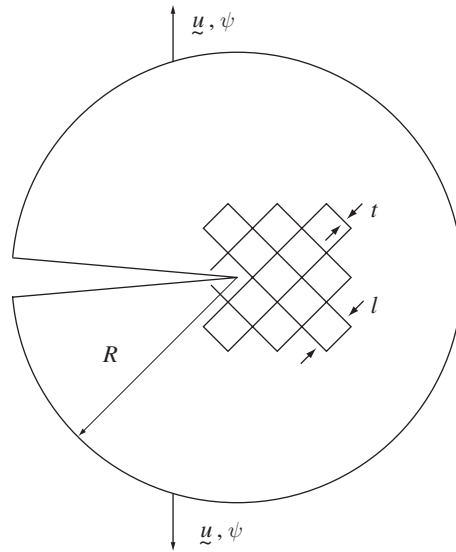


Figure 7. Boundary-layer analysis: lattice material with a macroscopic crack under K -control. The joint displacements and rotations associated with a K -field are prescribed on the outer boundary.

to as a boundary-layer analysis, was first employed by Schmidt & Fleck (2001) to investigate crack-growth initiation and subsequent propagation for regular and irregular elastic–plastic hexagonal lattices.

Fleck & Qiu (2006) have determined the fracture response of three elastic–brittle, isotropic lattices: hexagonal, triangular and Kagome (see figure 8). They found that the fracture toughness K_{IC} of these lattices scales with relative density $\bar{\rho}$ according to

$$\frac{K_{IC}}{\sigma_{TS}\sqrt{\ell}} = D\bar{\rho}^d, \quad (6.1)$$

where the exponent $d = 2$ for the hexagonal lattice, $d = 1$ for the triangular lattice and $d = 0.5$ for the Kagome lattice (see table 1).

It is emphasized that the value of the exponent d gives the sensitivity of fracture toughness to relative density. For example, at a relative density of 10%, the fracture toughness of the Kagome lattice is 10 times greater than that of the hexagonal lattice (see figure 8). The unusually high fracture toughness of the Kagome lattice is attributed to the presence of an elastic zone of bending emanating from the crack tip into a remote stretching field. The Kagome lattice exhibits pronounced crack-tip blunting due to the deformation band at the crack tip; this elastic blunting phenomenon reduces the stress levels at the crack tip and thereby increases the fracture toughness. Quintana Alonso & Fleck (2009) found a similar effect for the diamond-celled lattice. A particular feature of the diamond-celled lattice is a low resistance to shear along the $\pm 45^\circ$ directions; the elastic bending zones emanate from the crack tip along these directions. The high predicted value of fracture toughness for the Kagome lattice suggests that considerable benefits are achievable in ceramic cellular materials by use of such ideal micro-architectures.

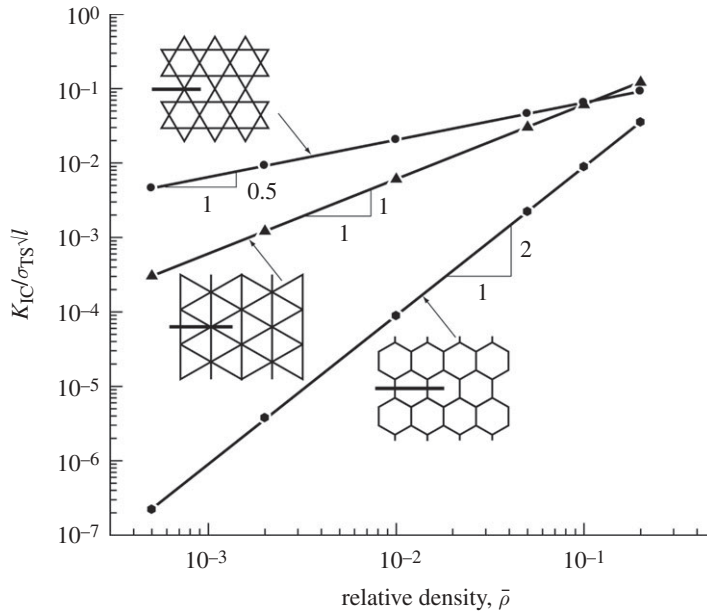


Figure 8. The predicted mode I fracture toughness K_{IC} plotted as a function of relative density $\bar{\rho} \propto t/\ell$, for the three isotropic lattices: hexagonal, triangular and Kagome.

We proceed to relate the fracture toughness K_{IC} of a lattice to the fracture toughness K_{IC}^S of the cell-wall material. Assume that the fracture strength σ_{TS} of the cell wall of a lattice material is dictated by the fracture toughness of the cell wall K_{IC}^S via an intrinsic flaw size a_0 , according to

$$\sigma_{TS} = \frac{K_{IC}^S}{\sqrt{\pi a_0}}. \quad (6.2)$$

Now substitute into (6.1) to obtain

$$\frac{K_{IC}}{K_{IC}^S} = D \bar{\rho}^d \left(\frac{\ell}{\pi a_0} \right)^{1/2}. \quad (6.3)$$

This expression is valid at low relative density. At high relative density, a more accurate expression would be

$$\frac{K_{IC}}{K_{IC}^S} = \bar{\rho}. \quad (6.4)$$

To obtain a single expression that attains both asymptotes, we introduce an arbitrary weight function $w(\bar{\rho})$, where

$$w(\bar{\rho}) = \exp \left(- \frac{\bar{\rho}}{(1 - \bar{\rho}) \bar{\rho}_0} \right). \quad (6.5)$$

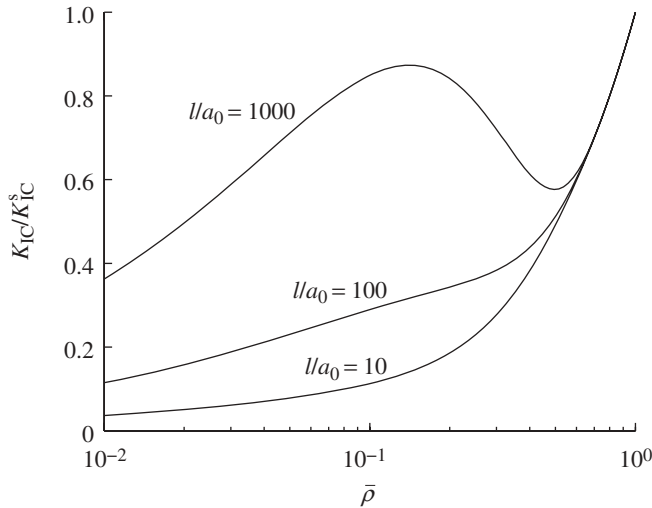


Figure 9. Predictions of the scaling of the fracture toughness of the Kagome lattice with relative density for three choices of the length scale ratio ℓ/a_0 and $\bar{\rho}_0 = 0.3$.

The parameter $\bar{\rho}_0$ can be interpreted to be the value of relative density at which the fracture toughness switches from the dilute lattice limit to that of a solid containing a dilute concentration of voids. Upon combining (6.3–6.5), we obtain

$$\frac{K_{IC}}{K_{IC}^S} = w(\bar{\rho}) D \bar{\rho}^d \left(\frac{\ell}{\pi a_0} \right)^{1/2} + (1 - w(\bar{\rho})) \bar{\rho}. \quad (6.6)$$

The weight function has the required asymptotic limits of $w(0) = 1$ and $w(1) = 0$ in order for (6.6) to reduce to (6.3) and to (6.4) when $\bar{\rho}$ equals 0 and 1, respectively. The relation (6.6) is plotted in figure 9 for three representative choices of the ratio ℓ/a_0 and the transition relative density $\bar{\rho}_0 = 0.3$. For high values of ℓ/a_0 , the fracture toughness of the lattice can be comparable to that of the parent solid material, even though the effective density of the lattice is 100 times less than the parent solid. This is primarily due to the discreteness of the lattice, i.e. the stress field deviates from the K -field solution at a distance of the order of ℓ from the crack tip, resulting in the enhanced fracture toughness. Figure 10 is a fracture toughness–density chart onto which this equation has been plotted for a Kagome lattice made of zirconia, ZrO_2 . It uses values for (D, d) from table 1, the values $K_{IC}^S = 7 \text{ MPa}\sqrt{\text{m}}$ and $\rho_s = 6000 \text{ kg m}^{-3}$ describing fully dense zirconia, and the parameter values $\ell/a_0 = 1000$ and $\bar{\rho}_0 = 0.3$. It illustrates the potential that architected materials, particularly those with the Kagome architecture, have for enabling the toughening of brittle materials.

The Kagome lattice has a remarkably high fracture toughness, such that K_{IC} scales with $\bar{\rho}^{1/2}$ for $\bar{\rho} \ll 1$. Upon recalling that the effective Young modulus of the lattice scales as $\bar{\rho}$, it follows that the toughness $G_{IC} = (1 - \nu^2) K_{IC}^2 / E$ of the lattice is independent of relative density. This is a remarkable result. But now a word of caution. All this is for the perfect lattice. Romijn & Fleck (2007) have shown that K_{IC} , and E , are imperfection sensitive for the Kagome lattice: upon

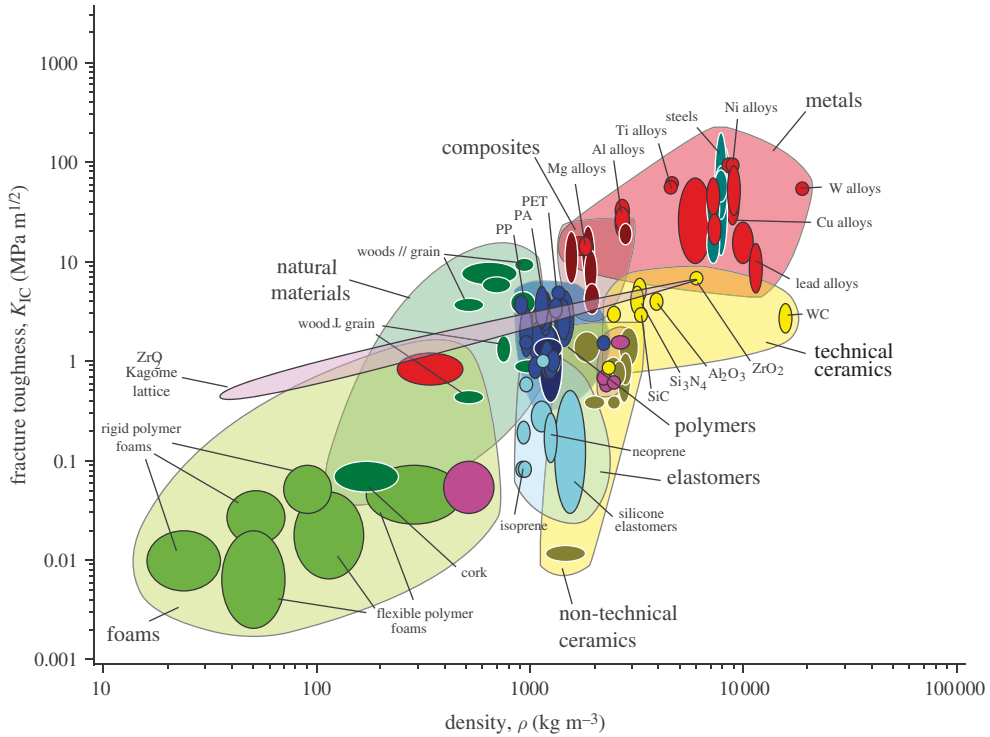


Figure 10. A plot of fracture toughness, K_{IC} , against density ρ for engineering materials. It shows how the fracture toughness of a zirconia Kagome lattice is predicted to evolve with density. At low densities, the lattice is far tougher than foams with a bending-dominated architecture. PET, polyethylene terephthalate; PA, polyamide; PP, polypropylene.

randomly repositioning nodes so that the microstructure is now stochastic in nature, the elastic shear bands emanating from the crack tip are disrupted and the crack-tip blunting mechanism is attenuated.

7. The damage tolerance of lattice materials

When a lattice material contains a short crack, its tensile strength is dictated by the tensile fracture strength of the lattice material σ_c . In contrast, when the lattice material contains a sufficiently long internal crack of length $2a$, its tensile strength is of order

$$\sigma = \frac{K_{IC}}{\sqrt{\pi a}} \quad (7.1)$$

in terms of the fracture toughness K_{IC} of the lattice material. A *transition flaw size* a_T can be identified immediately of magnitude

$$a_T = \frac{1}{\pi} \left(\frac{K_{IC}}{\sigma_c} \right)^2 = \frac{1}{\pi} \left(\frac{D}{C} \right)^2 \bar{\rho}^{2(d-c)} \ell \quad (7.2)$$

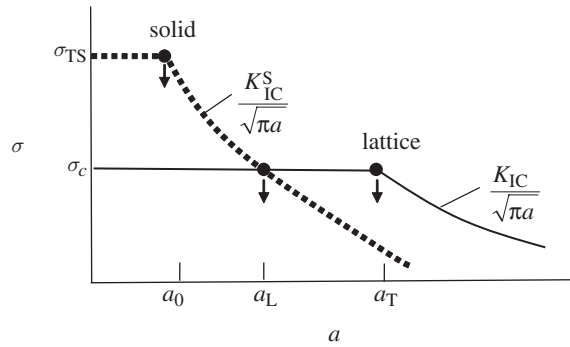


Figure 11. The damage tolerance of a lattice material and the parent solid.

upon making use of (4.6) and (6.1). Then, for a less than a_T , the lattice material is flaw insensitive and has a tensile strength close to σ_c , whereas for a greater than a_T , the tensile strength is dictated by the fracture toughness of the lattice (see figure 11).

It is instructive to compare the defect tolerance of an elastic-brittle lattice with that of the solid. Suppose the solid contains an internal crack of length $2a$. The dependence of tensile strength of the solid upon a is included in figure 11. For a less than the intrinsic flaw size a_0 , the tensile strength is given by $\sigma_{TS} = K_{IC}^S / \sqrt{\pi a_0}$, while for $a > a_0$, the tensile strength is given by $\sigma_{TS} = K_{IC}^S / \sqrt{\pi a}$. Consequently, a_0 serves the role of the transition flaw size for the solid.

We further note from figure 11 that the tensile strength of the defective lattice exceeds that of the parent solid provided the flaw size a is greater than a transition value

$$a_L = \frac{1}{\pi} \left(\frac{K_{IC}^S}{\sigma_c} \right)^2 = C^{-2} \bar{\rho}^{-2c} a_0 \quad (7.3)$$

via (4.6) and (6.2). Thus, for a triangulated lattice ($c=1$) of relative density $\bar{\rho} = 3\%$ and $C \approx 1$, we find that $a_L = 1000 a_0$. Typically, for ceramics, the intrinsic flaw size is of the order of $10 \mu\text{m}$, and so a_L is of the order of 10 mm . Thus, lattice materials compete with the parent solid in terms of damage tolerance for practical designs where flaws exist on the centimetre length scale. It is noteworthy that the transition flaw size a_L is sensitive to the relative density of the lattice, but not to the cell size ℓ .

8. Future directions

Lattice materials show promise for multi-functional applications, combining a mechanical function (such as stiffness and strength) with some other property (such as thermal or electrical conductivity), thereby making structural batteries, structural armour and deployable materials a possibility. Recently, it has been recognized that lattice materials have a morphing capability provided the parent pin-jointed lattice is statically and kinematically determinate (e. g. Hutchinson & Fleck 2006; Mai & Fleck 2009). This is a striking behaviour: when one of the bars of the lattice material is replaced by an actuator, the material is stiff

against external loads when the actuator is not triggered. However, when the actuator is deployed, the remaining structure can deform with minimal storage of internal energy. The two-dimensional Kagome lattice and its three-dimensional equivalent have particular promise, along with tubes of walls made from a fully triangulated lattice.

Multi-functional applications of lattice materials require combinations of properties, such as high stiffness and toughness at low density. Some progress has been made on the development of theoretical bounds for cross-property correlations (e.g. between thermal conductivity and stiffness), as reviewed by Milton (2002). However, there remains a need for a prescription of the appropriate two- or three-dimensional lattice architectures that lead to the desired *combination* of properties in material property space.

The theoretical methods for obtaining bounds on linear properties, such as modulus and thermal conductivity, are now well developed. Progress has also been made on the development of bounds for strength, but not for toughness. While strength is a bulk property, toughness is largely dictated by the weakest path of a crack. A wide range of toughening mechanisms exist in composites, including plasticity/internal friction, crack arrestors by crack-tip blunting, distributed microcracking and controlled fragmentation. A research challenge remains to optimize lattice materials for high toughness, yet maintain a high stiffness and strength, with low density.

References

- Ashby, M. F. 1991 On material and shape. *Acta Mater.* **39**, 1025–1039. (doi:10.1016/0956-7151(91)90189-8)
- Ashby, M. F. 2010 *Materials selection in mechanical design*, 4th edn. Oxford, UK: Butterworth–Heinemann.
- Ashby, M. F., Evans, A. G., Fleck, N. A., Gibson, L. J., Hutchinson, J. W. & Wadley, H. N. G. 2000 *Metal foams: a design guide*. Oxford, UK: Butterworth–Heinemann.
- Calladine, C. R. 1978 Buckminster Fuller's tensegrity structures and Clerk Maxwell's rules for construction of stiff frames. *Int. Solids Structs.* **14**, 161–172. (doi:10.1016/0020-7683(78)90052-5)
- Cundy, H. M. & Rolett, A. P. 1961 *Mathematical models*. Oxford, UK: Clarendon Press.
- Deshpande, V. S., Ashby, M. F. & Fleck, N. A. 2001a Effective properties of the octet-truss lattice material. *J. Mech. Phys. Solids* **49**, 1724–1769. (doi:10.1016/S0022-5096(01)00010-2)
- Deshpande, V. S., Ashby, M. F. & Fleck, N. A. 2001b Foam topology: bending versus stretching dominated architectures. *Acta Mater.* **49**, 1035–1040. (doi:10.1016/S1359-6454(00)00379-7)
- Fleck, N. A. & Qiu, X. 2006 The damage tolerance of elastic-brittle, two-dimensional isotropic lattices. *J. Mech. Phys. Solids* **55**, 562–588. (doi:10.1016/j.jmps.2006.08.004)
- Frederickson, G. N. 1997 *Dissections: plane and fancy*. Cambridge, UK: Cambridge University Press.
- Gibson, L. J. & Ashby, M. F. 1997 *Cellular solids. Structure and properties*, 2nd edn. Cambridge, MA: Cambridge University Press.
- Hutchinson, R. G. 2004 Mechanics of lattice materials. PhD thesis, Cambridge University, UK.
- Hutchinson, R. G. & Fleck, N. A. 2005 Micro-architected cellular solids—the hunt for statically determinate periodic trusses. *Z. Angew. Math. Mech.* **85**, 607–617. (doi:10.1002/zamm.200410208)
- Hutchinson, R. G. & Fleck, N. A. 2006 The structural performance of the periodic truss. *J. Mech. Phys. Solids* **54**, 756–782. (doi:10.1016/j.jmps.2005.10.008)
- Hyun, S. & Torquato, S. 2002 Optimal and manufacturable two-dimensional Kagome-like cellular solids. *J. Mater. Res* **17**, 137–144. (doi:10.1557/JMR.2002.0021)

- Lockwood, E. H. & Macmillan, R. H. 1978 *Geometric symmetry*. Cambridge, UK: Cambridge University Press.
- Mai, S. P. & Fleck, N. A. 2009 Reticulated tubes: effective elastic properties and actuation response. *Proc. R. Soc. A* **465**, 685–708. (doi:10.1098/rspa.2008.0328)
- Milton, G. 2002 *The theory of composites*. Cambridge, UK: Cambridge University Press.
- Pellegrino, S. & Calladine, C. R. 1986 Matrix analysis of statically and kinematically indeterminate frameworks. *Int. Solids Structs.* **22**, 409–428. (doi:10.1016/0020-7683(86)90014-4)
- Quintana Alonso, I. & Fleck, N. A. 2009 Compressive response of a sandwich plate containing a cracked diamond-celled lattice. *J. Mech. Phys. Solids* **57**, 1545–1567. (doi:10.1016/j.jmps.2009.05.008)
- Romijn, N. E. R. & Fleck, N. A. 2007 The fracture toughness of planar lattices: imperfection sensitivity. *J. Mech. Phys. Solids* **55**, 2538–2564. (doi:10.1016/j.jmps.2007.04.010)
- Schmidt, I. & Fleck, N. A. 2001 Ductile fracture of two-dimensional foams. *Int. J. Fracture* **111**, 327–342. (doi:10.1023/A:1012248030212)
- Syozii, I. 1972 Transformation of Ising models. In *Phase transitions and critical phenomena* (eds C. Domb & M. S. Green). New York, NY: Academic Press.
- Wadley, H. N. G., Fleck, N. A. & Evans, A. G. 2003 Fabrication and structural performance of periodic cellular metal sandwich structures. *Comp. Sci. Tech.* **63**, 2331–2343. (doi:10.1016/S0266-3538(03)00266-5)